# Simultaneous X-Ray, Gamma-Ray, and Radio Observations of the Repeating Fast Radio Burst FRB 121102

P. Scholz[1], S. Bogdanov[2], J. W. T. Hessels[3,4], R. S. Lynch[5,6], L. G. Spitler[7], C. G. Bassa[3], G. C. Bower[8],
S. Burke-Spolaor[6,9], B. J. Butler[9], S. Chatterjee[10], J. M. Cordes[10], K. Gourdji[4], V. M. Kaspi[11], C. J. Law[12],
B. Marcote[13], M. A. McLaughlin[6], D. Michilli[3,4], Z. Paragi[13], S. M. Ransom[14],
A. Seymour[15], S. P. Tendulkar[11], and R. S. Wharton[10]

[1] National Research Council of Canada, Herzberg Astronomy and Astrophysics, Dominion Radio Astrophysical Observatory,
P.O. Box 248, Penticton, BC V2A 6J9, Canada; paul.scholz@nrc-cnrc.gc.ca
[2] Columbia Astrophysics Laboratory, Columbia Univ., New York, NY 10027, USA
[3] ASTRON, The Netherlands Institute for Radio Astronomy, Postbus 2, 7990 AA Dwingeloo, The Netherlands
[4] Anton Pannekoek Institute for Astronomy, University of Amsterdam, Science Park 904, 1098 XH Amsterdam, The Netherlands
[5] Green Bank Observatory, P.O. Box 2, Green Bank, WV 24944, USA
[6] Center for Gravitational Waves and Cosmology, Dept. of Physics and Astronomy, West Virginia University, White Hall,
Box 6315, Morgantown, WV 26506, USA
[7] Max-Planck-Institut für Radioastronomie, Auf dem Hügel 69, D-53121 Bonn, Germany
[8] Academia Sinica Institute of Astronomy and Astrophysics, 645 N. A'ohoku Place, Hilo, HI 96720, USA
[9] National Radio Astronomy Observatory, Socorro, NM 87801, USA
[10] Dept. of Astronomy and Cornell Center for Astrophysics and Planetary Science, Cornell University, Ithaca, NY 14853, USA
[11] Dept. of Physics and McGill Space Institute, McGill University, Montreal, QC H3A 2T8, Canada
[12] Department of Astronomy and Radio Astronomy Lab, University of California, Berkeley, CA 94720, USA
[13] Joint Institute for VLBI ERIC, Postbus 2, 7990 AA Dwingeloo, The Netherlands
[14] National Radio Astronomy Observatory, Charlottesville, VA 22903, USA
[15] Arecibo Observatory, HC3 Box 53995, Arecibo, PR 00612, USA

## Abstract

We undertook coordinated campaigns with the Green Bank, Effelsberg, and Arecibo radio telescopes during *Chandra X-ray Observatory* and *XMM-Newton* observations of the repeating fast radio burst FRB 121102 to search for simultaneous radio and X-ray bursts. We find 12 radio bursts from FRB 121102 during 70 ks total of X-ray observations. We detect no X-ray photons at the times of radio bursts from FRB 121102 and further detect no X-ray bursts above the measured background at any time. We place a $5\sigma$ upper limit of $3 \times 10^{-11}$ erg cm$^{-2}$ on the 0.5–10 keV fluence for X-ray bursts at the time of radio bursts for durations <700 ms, which corresponds to a burst energy of $4 \times 10^{45}$ erg at the measured distance of FRB 121102. We also place limits on the 0.5–10 keV fluence of $5 \times 10^{-10}$ and $1 \times 10^{-9}$ erg cm$^{-2}$ for bursts emitted at any time during the *XMM-Newton* and *Chandra* observations, respectively, assuming a typical X-ray burst duration of 5 ms. We analyze data from the *Fermi Gamma-ray Space Telescope* Gamma-ray Burst Monitor and place a $5\sigma$ upper limit on the 10–100 keV fluence of $4 \times 10^{-9}$ erg cm$^{-2}$ ($5 \times 10^{47}$ erg at the distance of FRB 121102) for gamma-ray bursts at the time of radio bursts. We also present a deep search for a persistent X-ray source using all of the X-ray observations taken to date and place a $5\sigma$ upper limit on the 0.5–10 keV flux of $4 \times 10^{-15}$ erg s$^{-1}$ cm$^{-2}$ ($3 \times 10^{41}$ erg s$^{-1}$ at the distance of FRB 121102). We discuss these non-detections in the context of the host environment of FRB 121102 and of possible sources of fast radio bursts in general.

*Key words:* gamma rays: general – stars: neutron – X-rays: bursts – X-rays: general

## 1. Introduction

Fast radio bursts (FRBs) are a recently discovered (Lorimer et al. 2007; Thornton et al. 2013) class of radio transient that have as yet unclear physical origins. They are short (durations of milliseconds), bright (peak flux densities ∼0.1–10 Jy at 1–2 GHz) bursts that appear to be coming from outside of the Galaxy based on their high dispersion measures (DMs). Their implied distances, based on the DM excesses in comparison to the expected line-of-sight contributions from our Galaxy (Cordes & Lazio 2002; Yao et al. 2017) suggest that they come from cosmological redshifts (i.e., $z \gtrsim 0.5$; Thornton et al. 2013). To date, 23 FRB sources have been discovered, 17 of which have been found with the Parkes Telescope, one each at the Arecibo and Green Bank Telescopes (GBT; Spitler et al. 2014; Masui et al. 2015), three using the UTMOST array (Caleb et al. 2017), and one at the Australian Square Kilometre Array Pathfinder (Bannister et al. 2017). See Petroff et al. (2016) for a catalog of published FRBs.[16]

The first FRB discovered at a telescope other than Parkes was FRB 121102 (Spitler et al. 2014) at the 305 m Arecibo telescope in the PALFA Survey (Cordes et al. 2006; Lazarus et al. 2015). Follow-up observations of FRB 121102 revealed additional bursts from a location and DM consistent with the original burst (Spitler et al. 2016). This showed that FRB 121102 cannot be explained by cataclysmic models (e.g., Kashiyama et al. 2013; Falcke & Rezzolla 2014), though this may not be true of all FRBs. Strong arguments were also made for the extragalactic nature of FRB 121102 based on the lack of any evidence for any Galactic H II region to provide the excess dispersing plasma (Scholz et al. 2016).

---

[16] http://www.astronomy.swin.edu.au/pulsar/frbcat/

**Table 1**
Summary of Joint X-Ray/Radio Observations

| Telescope | Obs ID/ Proj. Code | Start Time (UTC) | End Time (UTC) | Exposure Time (s) |
|---|---|---|---|---|
| *XMM-Newton* | 0792382801 | 2016 Sep 16 00:39:57 | 2016 Sep 16 06:21:37 | 13490 |
| | 0792382901 | 2016 Sep 17 23:59:20 | 2016 Sep 18 06:31:00 | 15621 |
| *Chandra* | 19286 | 2016 Nov 26 01:12:24 | 2016 Nov 26 07:36:48 | 20810 |
| | 19287 | 2017 Jan 11 22:33:22 | 2017 Jan 12 04:44:43 | 19820 |
| GBT | GBT16B-391 | 2016 Sep 16 03:59:12 | 2016 Sep 16 08:00:04 | 14452 |
| | | 2016 Sep 18 04:02:15 | 2016 Sep 18 08:00:04 | 14269 |
| | CH18500414 | 2016 Nov 26 02:06:46 | 2016 Nov 26 07:30:04 | 19398 |
| | | 2017 Jan 11 23:13:56 | 2017 Jan 12 04:45:05 | 19869 |
| Effelsberg | | 2016 Sep 16 04:04:06 | 2016 Sep 16 07:04:24 | 10818 |
| Arecibo | P3054 | 2017 Jan 12 01:46:27 | 2017 Jan 12 03:30:57 | 6270 |

The extragalactic nature was confirmed when a direct sub-arcsecond localization of the repeating bursts was achieved from Karl G. Jansky Very Large Array (VLA) observations in late 2016 (Chatterjee et al. 2017) and a host galaxy was identified. Using optical imaging and spectroscopy with the Gemini and Keck telescopes, the host was found to be a faint, low-metallicity, star-forming, dwarf galaxy with a redshift of $z = 0.193$ (implying a luminosity distance of 972 kpc; Tendulkar et al. 2017). The VLA observations also showed that the source of FRB 121102 is coincident with a 0.2 mJy persistent radio source and European VLBI Network (EVN) observations further showed that the persistent source is compact to $\lesssim 0.2$ mas ($\lesssim 0.7$ pc, given the host distance) and that the bursts come from within $\lesssim 12$ mas ($\lesssim 40$ pc) of the persistent source (Marcote et al. 2017). Using *Hubble Space Telescope* observations, Bassa et al. (2017) resolved the host galaxy and showed that the burst and persistent radio source is located in a bright star-forming region on the outskirts of the galaxy. Though they are co-located, and thus very likely share some kind of physical or evolutionary relationship, the persistent source and the source of radio bursts do not necessarily need to be one and the same.

Many models have been proposed for FRBs (for a review see Katz 2016a). The extreme luminosities and short duration of FRBs point to coherent emission originating from a compact object. Two classes of known phenomena that emit repeated radiation on those timescales are X-ray/gamma-ray bursts from magnetars (Popov & Postnov 2013) and giant pulses from radio pulsars (Pen & Connor 2015; Cordes & Wasserman 2016). The identification of the host galaxy of FRB 121102 as a low-metallicity dwarf (Tendulkar et al. 2017), as well as the source's projected location in a star-forming region (Bassa et al. 2017) bolsters the case for the possible magnetar nature of the source, as these galaxies are preferentially hosts to long gamma-ray bursts and hydrogen-poor superluminous supernovae (SLSNe-I), which are thought to result in the birth of magnetars (Lunnan et al. 2014). The nature of the persistent source in this model would be a pulsar wind nebula (PWN) driven by the young magnetar (Kashiyama & Murase 2017) or an interaction of the supernova blast wave with surrounding progenitor wind bubble (Metzger et al. 2017).

Known Galactic magnetars produce both X-ray and gamma-ray bursts/flares and radio pulsations on timescales of a few to hundreds of milliseconds, similar to the durations of FRB radio bursts. Lyutikov (2002) estimates a ratio of radio-to-X-ray

energy emitted in such bursts of $10^{-4}$ based on analogies to solar flares. The model of Lyubarsky (2014) where a synchrotron maser is produced from a magnetized shock, predicts $10^{-5}$–$10^{-6}$. Given the energies of radio bursts of FRBs, $\sim 10^{39}$–$10^{41}$ erg, these models predict X-ray energies of $\sim 10^{43}$–$10^{47}$ erg, which may be detectable by X-ray and gamma-ray telescopes.

Here, we present a campaign of simultaneous X-ray and radio observations in late 2016 and early 2017 with the goal of detecting or constraining any X-ray counterparts to the radio bursts from FRB 121102. This improves on previous X-ray burst searches (e.g., Scholz et al. 2016), which were not simultaneous and thus sub-optimal for probing coincident X-ray bursts. In Section 2, we describe the observations performed. In Section 3, we present the results of our search for radio (Arecibo, Green Bank, and Effelsberg Telescopes), X-ray (*Chandra* and *XMM-Newton*), and gamma-ray (*Fermi*) bursts during the coordinated campaign as well as limits on a persistent X-ray source. We discuss the significance of these results in Section 4.

## 2. Observations

In 2016 September and November and 2017 January, we undertook coordinated observations between radio telescopes, namely the Green Bank, Arecibo, and Effelsberg telescopes, and the *XMM-Newton* and *Chandra* X-ray telescopes. Table 1 and Figure 1 summarize the observations presented here and their overlap. In all cases, the telescopes were pointed at the position of FRB 121102, R.A. = $05^h 31^m 58^s.701$, decl. = $+33°08'52''.55$ (Marcote et al. 2017). This position was also used to correct the arrival times of the data to the solar system barycenter (SSB). For all data sets, the DE405 solar system ephemeris was used for barycentric corrections.

### 2.1. Green Bank Telescope

The 110 m Robert C. Byrd GBT observed FRB 121102 on 2016 September 16, 18, November 26, and 2017 January 11 during periods that overlapped with either *XMM-Newton* or *Chandra* observations (Table 1; Figure 1). FRB 121102 was observed with the S-band receiver at a center frequency of 2 GHz and a bandwidth of 800 MHz, of which about 600 MHz is usable due to receiver roll-off and the masking of spectral channels containing radio frequency interference (RFI). We used the Green Bank Ultimate Pulsar Processing Instrument
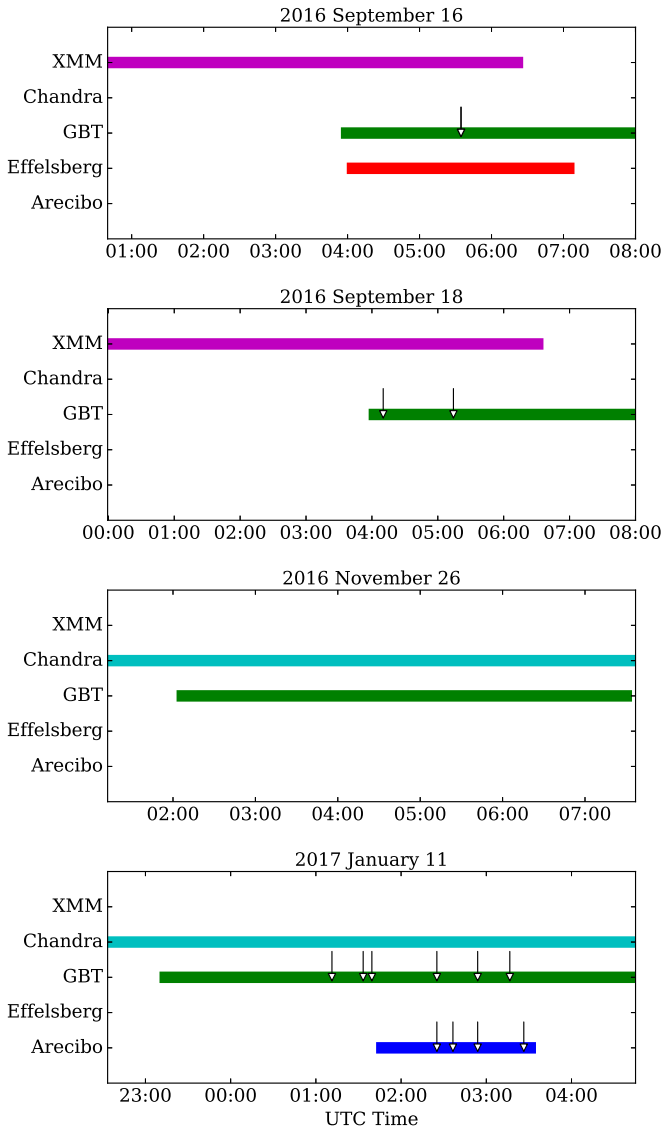
**Figure 1.** Timelines of overlapping radio and X-ray observations. Each bar represents the time when each telescope was observing. The arrows mark the times of detected bursts. Note that GBT bursts 1 and 2 are only ~40 ms apart (see Figure 2) and so appear as a single arrow. Note that we only present the radio burst detections that have simultaneous X-ray coverage in this work.

(GUPPI; DuPlain et al. 2008) in coherent de-dispersion mode where each of the spectral channels were corrected for dispersion in real time to DM = 557 pc cm$^{-3}$. These coherently de-dispersed observations therefore do not suffer from intra-channel DM smearing, as the correction is performed before Stokes parameters are formed. This mode provides full Stokes parameters, 512 spectral channels (each 1.56 MHz wide), and a time resolution of 10.24 $\mu$s.

### 2.2. Effelsberg Telescope

The 100 m Effelsberg telescope performed a three hour observation of FRB 121102 on 2016 September 16, simultaneous with both the GBT and *XMM-Newton* observations (Table 1). Data were recorded at 1.4 GHz with an observing configuration that was identical to what is used for the HTRU-N pulsar and fast transient survey. Details can be found in Barr et al. (2013). FRB 121102 was observed with the central pixel of the 7-beam

L-band receiver and data were recorded with the PFFTS pulsar search mode backends. The data cover a frequency range of 1210–1510 MHz with 512 frequency channels and have a time resolution of 54.613 $\mu$s. Note, unlike the GBT and Arecibo observations, these data were not coherently de-dispersed and so suffer from ~1 ms of intra-channel DM smearing at the DM of FRB 121102.

### 2.3. Arecibo Telescope

The 305 m William E. Gordon Telescope at Arecibo Observatory observed FRB 121102 on 2017 January 12 simultaneously with GBT and *Chandra* observations (Table 1). We used the single-pixel L-wide receiver with the Puerto Rican Ultimate Pulsar Processing Instrument (PUPPI) backend. This setup provided 800 MHz of bandwidth centered at 1380 MHz, of which about 600 MHz is usable due to receiver roll-off and RFI excision. As with GUPPI, the data were coherently de-dispersed to DM = 557 pc cm$^{-3}$ in real time with 512 spectral channels (each 1.56 MHz wide) and a time resolution of 10.24 $\mu$s.

### 2.4. XMM-Newton

Two *XMM-Newton* Director's Discretionary Time (DDT) observations were performed on 2016 September 16 and 18 (Table 1). These DDT observations were scheduled in response to a period of high radio burst activity, with several bursts detected per hour (Chatterjee et al. 2017; Law et al. 2017). We used the EPIC/pn camera in Small Window mode (5.7 ms time resolution) and the EPIC/MOS cameras in Timing mode (1.75 ms time resolution). The Timing mode observations provide only one dimension of spatial information, which results in a high background (see Section 3.2).

Unfortunately, the pn-mode observations have a deadtime fraction of 29%. This means that for every 5.7 ms frame of the pn observation, the telescope is blind to X-ray photons for 1.65 ms. Though this time resolution is helpful in resolving bursts when a significant number of counts are detected, the deadtime is detrimental when placing a limit following a non-detection. We therefore do not use the pn-mode data below when placing fluence limits for putative X-ray bursts.

Standard tools from the *XMM-Newton* Science Analysis System (SAS) version 16.0 and HEASoft version 6.19 were used to reduce the data. For each observation, the raw Observation Data Files (ODF) level data were downloaded and were pre-processed using the SAS tools *emproc* and *epproc*. Data were filtered so that single-quadruple events with energies between 0.1–12 keV (pn) and 0.2–15 keV (MOS) were retained, and standard "FLAG" filtering was applied. The light curves were then inspected for soft proton flares and none were found. Event arrival times were then corrected to the SSB. For the pn, we extracted source events from an 18″ radius (80% encircled energy) source region centered on the position of FRB 121102. For the MOS cameras, we extracted events from a 20 pixel (22″) wide strip centered on the position of the source.

### 2.5. Chandra X-Ray Observatory

The *Chandra X-ray Observatory* targeted FRB 121102 on 2016 November 26 (ObsID 19286) and 2017 January 11 (ObsID 19287) using the front-illuminated ACIS-I instrument for 20 ks in both instances. The detector was operated in VFAINT mode with the entire array read out using a 3.2 s

frame time. These observations were part of a joint *Chandra*/ GBT Cycle 18 project to obtain contemporaneous data with the two telescopes.

The resulting *Chandra* data sets were analyzed using CIAO[17] version 4.8.2 (Fruscione et al. 2006) following standard procedures recommended by the *Chandra* X-ray Center. We extracted events from a $1''$ radius region (95% encircled energy) centered on the position of FRB 121102 and corrected the photon arrival times to the SSB using the aforementioned source position.

## 3. Analysis and Results

### 3.1. Radio Bursts

The radio observations from GBT, Effelsberg, and Arecibo were searched for bursts using standard tools in the PRESTO[18] (Ransom 2001) software package. For the purposes of searching, the data were downsampled by a factor of 8 (to a time resolution of 81.92 $\mu$s) for Arecibo and GBT observations and a factor of 16 (874 $\mu$s resolution) for Effelsberg observations. We first used 'rfifind' to identify frequency and time blocks contaminated by RFI, which were masked in the subsequent search. The data were then de-dispersed in a DM range of 507–607 pc cm$^{-3}$ with step size 0.5 pc cm$^{-3}$ for GBT, 535–585 pc cm$^{-3}$ with a step size of 1 pc cm$^{-3}$ for Effelsberg, and 527–626 pc cm$^{-3}$ with a step size of 1 pc cm$^{-3}$ for Arecibo. Burst candidates were identified in a boxcar matched filtering search for pulse widths up to 20 ms and S/N > 5 using 'single_pulse_search.py'. Due to the effects of RFI, our search is only complete in the Arecibo observation to S/N $\gtrsim$ 13 and to S/N $\gtrsim$ 7 for Effelsberg and GBT.

Four astrophysical bursts at a DM consistent with that of FRB 121102 were found in the GBT observations on 2016 September 16 and 18 at times that overlapped with the simultaneous *XMM-Newton* observations (labeled, in this work, as bursts GBT 1–4). Radio bursts at times outside of the simultaneous X-ray coverage are not presented here. Five more bursts were found in the GBT observation on 2017 January 11 that overlapped with the *Chandra* observation (bursts GBT 5–7, 9, and 10). Three bursts were found in the search of the 2017 January 11 Arecibo observation (AO 1, 2, and 4). During one of the detected GBT bursts (GBT 9) a coincident burst (AO 3) was found in the Arecibo observation when searching specifically at the time of burst GBT 9, which was otherwise missed due to RFI. Similarly, burst GBT 8 was found at the time of burst AO 1. The remainder of the GBT- and Arecibo-detected bursts were not detected in the corresponding other telescope. To summarize, a total of 12 radio bursts were found with two co-detections (GBT 8/AO 1 and GBT 9/AO 3).

In the Effelsberg observation on 2016 September 16, all events with S/N > 7 can be attributed to RFI. Because these observations overlap with the times of GBT-detected bursts, the three second windows around the arrival times of the coincident GBT bursts were searched manually, using a range of downsample factors, but no bursts were identified. These contemporaneous non-detections, as well as those during the 2017 January 11 Arecibo and GBT observations that did not result in co-detections, are likely due to the narrow-band nature

of FRB 121102 radio bursts (see Scholz et al. 2016; Spitler et al. 2016).

The GBT-detected radio bursts are shown in Figure 2, and those detected at Arecibo are shown in Figure 3. We show only the time series for each burst and defer a full spectral analysis of the bursts to a future work. For each burst, we measured the peak flux density, fluence, and burst width (Gaussian FWHM) using an identical procedure to Scholz et al. (2016). These values are shown in Table 2. We note that bursts GBT 1 and 2 arrived ∼40 ms apart. This is the minimum separation reported thus far for radio bursts from FRB 121102. This does not necessarily imply an upper limit to an underlying periodicity of <40 ms, as we cannot exclude the possibility that this is a single wide burst with multiple peaks, or if the source is a rotating object that multiple bursts were emitted from during a single rotation. We defer a more detailed analysis of the arrival times to a future work with a much larger sample of bursts. The measured radio burst arrival times were corrected to the SSB and corrected for the dispersive delay to infinite frequency using DM = 559 pc cm$^{-3}$ (Scholz et al. 2016; which is more accurately measured than the DM = 557 pc cm$^{-3}$ used during data collection, see Section 2) and are therefore directly comparable to the SSB-referenced arrival times of the X-ray photons.

### 3.2. Limit on X-Ray Burst Emission

For each detected radio burst, we searched nearby in time for X-ray photons that could be due to X-ray bursts. In the 2016 September 16 *XMM-Newton* observation, the closest photon to Bursts 1 and 2 was 5.8 s away. The false alarm probability for an event to arrive in such a window given the 0.5–10 keV background count rate of 0.01 counts s$^{-1}$ is 25%. In the 2016 September 18 *XMM-Newton* observation, no photons were closer than 0.7 s from a radio burst (background count rate 0.05 counts s$^{-1}$, false alarm probability 13%). In the 2017 January 11 *Chandra* observation, a single photon was detected at the source position and was 893 s away from the closest radio burst (background count rate $5 \times 10^{-5}$ counts s$^{-1}$, false alarm probability 42%). Given the high probability that these are background events, we have no reason to think they are related to FRB 121102. For each observation, the total number of X-ray counts detected within the source extraction region of FRB 121102 was consistent with the background count rate.

For both *XMM-Newton* and *Chandra* observations, we also performed a similar exercise as above with the raw event lists (Level 1 for *Chandra* and ODF-level for *XMM-Newton*) prior to applying any standard filtering in case a bright X-ray burst was flagged as a cosmic ray. There was no evidence for any X-ray events in excess of the unfiltered background count rate.

We place a limit on the number of X-ray counts from FRB 121102 using the Bayesian method of Kraft et al. (1991). For a putative X-ray burst at the time of a detected radio burst, we can place an upper limit of 14.4 counts at a $5\sigma$ confidence limit in 0.5–10 keV. This limit is independent of duration up to the time of the nearest detected photon (see above), because the background is negligible. For an X-ray burst arriving outside of this window at any time during the observation, the background rate and trials factor depend on the assumed duration. So, we assume a duration of 5 ms, similar to that of the radio bursts, which leads to a 0.5–10 keV count limit of 32.3 counts during the *XMM-Newton* observations and 33.8 counts for *Chandra* ($5\sigma$ confidence).

---
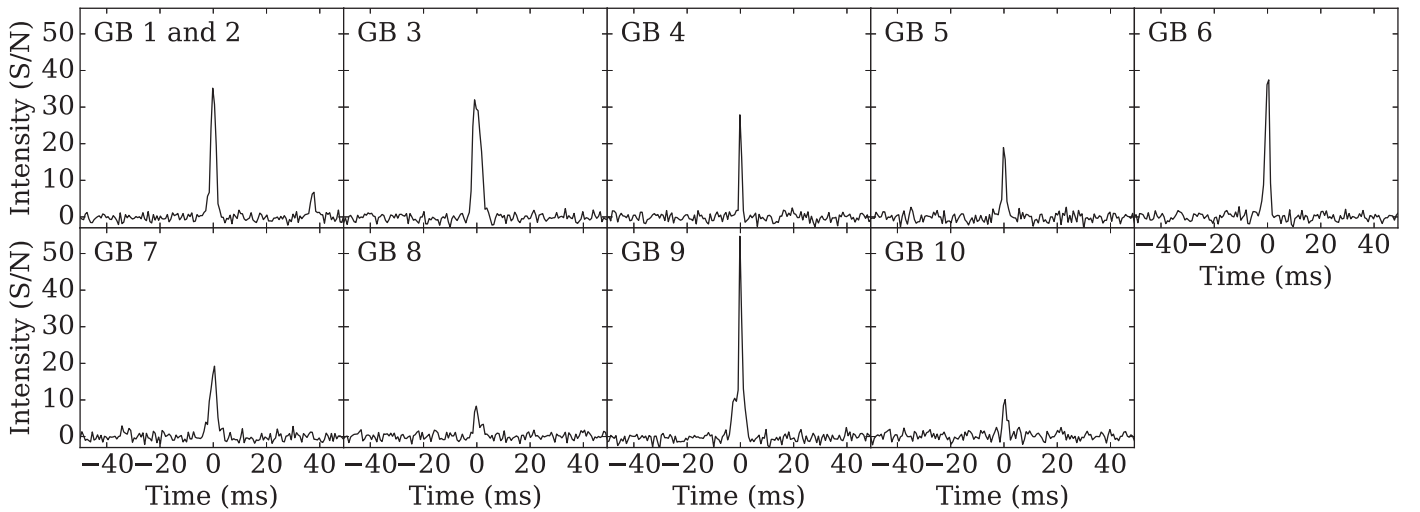
**Figure 2.** Time series for each GBT burst that occurred during the *XMM-Newton* and *Chandra* observations. Each burst has been de-dispersed to 559 pc cm$^{-3}$ to be consistent with the measured average DM in Scholz et al. (2016). Each time series has been downsampled to a time resolution of 655.36 $\mu$s.

A count limit, $\mu_{\mathrm{lim}}$ can be translated to a fluence limit by dividing by a spectrally averaged effective area for the instrument, $A$, and multiplying by an average photon energy, $E$. We can also stack individual limits, under the assumption that X-ray bursts with similar spectra are emitted at the times of every radio burst. In the case where zero counts are detected in each detector (i.e., *XMM-Newton*/MOS and *Chandra*/ACIS) and the background count rate is negligible, the count rate limit is simply $\mu_{\mathrm{lim}} = -\log(1 - \mathrm{CL})$, where CL is the desired confidence level (in our case 0.9999994 for 5$\sigma$), and the fluence limit takes the form,

$$F_{\mathrm{lim}} = \frac{\mu_{\mathrm{lim}}}{\sum_i \frac{N_i A_i}{E_i}}. \tag{1}$$

Here, the sum is over each instrument, which have each observed simultaneously during $N_i$ radio bursts. We read the effective area of each telescope as a function of energy from the ancillary response files for each telescope.[19] Using these effective area curves, in Figure 5, we plot the limiting burst energy as a function of photon energy. Here, we derive a model-independent limit where there is an equal probability of a source photon occurring across the entire band. The 5$\sigma$ confidence upper limit on the 0.5–10 keV fluence for a single X-ray burst at the time of one of the detected radio bursts is $2 \times 10^{-10}$ erg cm$^{-2}$ for observations simultaneous with *XMM-Newton* and $5 \times 10^{-10}$ erg cm$^{-2}$ for *Chandra*, or $3 \times 10^{46}$ erg and $6 \times 10^{46}$ erg at the luminosity distance of FRB 121102, respectively. If we additionally assume that X-ray bursts of similar fluence are emitted at the time of every radio burst (i.e., stacked as per Equation (1)), the upper limit at the time of the bursts becomes $3 \times 10^{-11}$ erg cm$^{-2}$ ($4 \times 10^{45}$ erg at the source distance). The limit for an X-ray burst arriving at any time during the X-ray observations is $5 \times 10^{-10}$ erg cm$^{-2}$ for *XMM-Newton* and $1 \times 10^{-9}$ erg cm$^{-2}$ for *Chandra* for an assumed duration of 5 ms (which correspond to energy limits of $6 \times 10^{46}$ and $1 \times 10^{47}$ erg).

---

[19] From http://cxc.harvard.edu/caldb/prop_plan/imaging/index.html for *Chandra*/ACIS, http://xmm2.esac.esa.int/external/xmm_sw_cal/calib/epic_files.shtml for *XMM-Newton*/EPIC.

### 3.3. Limit on Gamma-Ray Burst Emission

We also searched data from the *Fermi* Gamma-ray Burst Monitor (GBM; Meegan et al. 2009) for gamma-ray burst counterparts during the radio bursts presented in this work. FRB 121102 was only visible to GBM during the 2016 September *XMM-Newton*/GBT observations, and so our limit applies only to those four bursts. In an analysis similar to what has been done for previous FRB 121102 radio bursts (Younes et al. 2016), we used the Time Tagged Event GBM data in the energy range 10–100 keV and searched for excess counts in 1 and 5 ms bins in 2 s windows centered on the arrival time of the four radio bursts. We find no signals that are not attributable to Poisson fluctuations from the background count rate at a 5$\sigma$ confidence level. Taking into account the effective area of *Fermi*/GBM at 10–100 keV, the background count rate, and a typical photon energy of 40 keV, we place an upper limit of $1 \times 10^{-8}$ erg cm$^{-2}$ for each burst and $4 \times 10^{-9}$ erg cm$^{-2}$ if we assume a gamma-ray burst is emitted at the time of each radio burst, which, at the measured luminosity distance, corresponds to a 10–100 keV burst energy limit of $5 \times 10^{47}$ erg.

### 3.4. Limit on Persistent X-Ray Source

In order to probe more deeply for faint emission from a persistent X-ray source at the location of FRB 121102 than previous limits (Scholz et al. 2016; Chatterjee et al. 2017), we produced a summed image of all the *Chandra* data to date. We co-added, aspect-corrected, and exposure-corrected the two ACIS-I exposures from our 2016 November and 2017 January observations along with the ACIS-S exposure previously presented in Scholz et al. (2016) using the merge_obs script in CIAO. In the combined 80 ks exposure, only two events are registered within an aperture of radius 1″ centered on the position of FRB 121102 (see Figure 4), entirely consistent with being due to background emission. We measure a 0.5–10 keV background count rate in a 40″ radius region away from the source to be 0.20 counts s$^{-1}$ sq. arcsec$^{-1}$. Using the number of detected counts and measured background rate, we place a count rate limit using the Bayesian method of Kraft et al. (1991) and translate it to a flux using the same method as in the burst case (Section 3.2). Assuming a photoelectrically absorbed
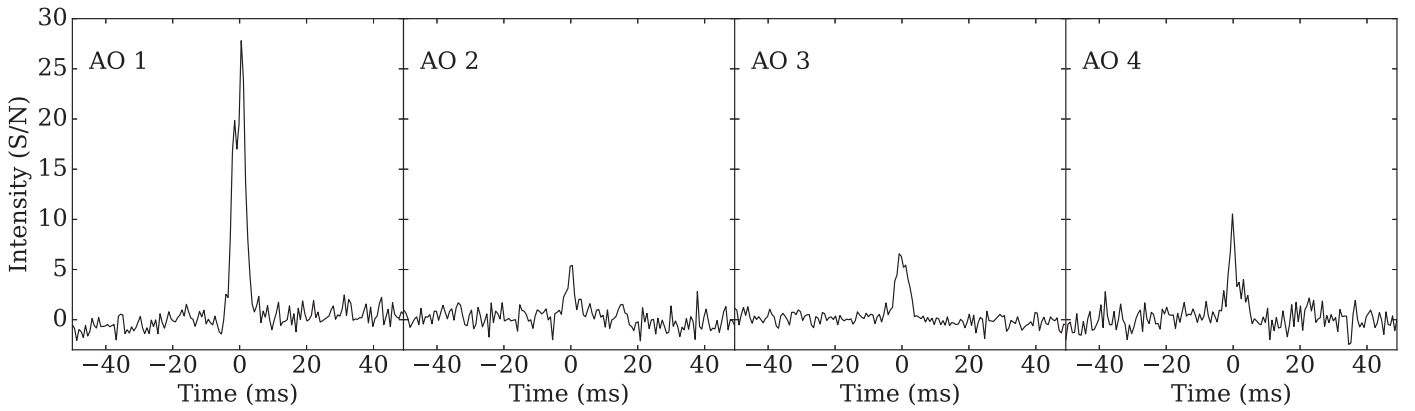
**Figure 3.** Time series for each Arecibo-detected burst that occurred during the *Chandra* observation on 2017 January 12. Each burst has been de-dispersed to 559 pc cm$^{-3}$ to be consistent with the measured average DM in Scholz et al. (2016). Each time series has been downsampled to a time resolution of 655.36 $\mu$s.

power-law source spectrum with a spectral index of $\Gamma = 2$ and a hydrogen column density of $N_{\mathrm{H}} \sim 1.7 \times 10^{22}$ cm$^{-2}$ (as in Chatterjee et al. 2017), the $5\sigma$ upper limit on any persistent 0.5–10 keV X-ray emission from FRB 121102 or the host galaxy is $4 \times 10^{-15}$ erg cm$^{-2}$ s$^{-1}$. As the *XMM-Newton* data presented in this work were included for the persistent X-ray source limit in Chatterjee et al. (2017), their value of $5 \times 10^{-15}$ erg cm$^{-2}$ s$^{-1}$ is still valid for the *XMM-Newton* images.

## 4. Discussion

From the non-detections of X-ray photons at the times of radio bursts from FRB 121102, we have placed a 0.5–10 keV X-ray burst energy limit of $4 \times 10^{45}$ erg assuming an X-ray burst emitted at the time of every radio burst. If we search for bursts at any time during X-ray observations of FRB 121102 we can place a 0.5–10 keV X-ray energy limit of $6 \times 10^{46}$ erg and $1 \times 10^{47}$ erg for *XMM-Newton* and *Chandra* observations, respectively, assuming a burst duration of 5 ms. These model-independent limits, however, assume an equal probability of source photons arriving across the entire 0.5–10 keV band and do not take into account the effects of photoelectric absorption. These limits, therefore, can change significantly depending on the assumed spectral model and come with several caveats, which we will explore here.

### 4.1. Effect of Source Models and Caveats

Potential sources of X-ray bursts that accompany FRBs can have different underlying spectra. Here, we explore the effect of different source spectra on the fluence limits. To generate the assumed source spectra, we use XSPEC v12.9.0n, using abundances from Wilms et al. (2000) and photoelectric cross-sections from Verner et al. (1996) for $N_{\mathrm{H}}$.

We initially estimate the $N_{\mathrm{H}}$ to the source from the DM–$N_{\mathrm{H}}$ relation of He et al. (2013). We take the DM contribution from our Galaxy to be 188 pc cm$^{-3}$ (from the NE2001 model of Cordes & Lazio 2002). The DM of the host has been estimated to be $55 \lesssim \mathrm{DM}_{\mathrm{host}} \lesssim 225$ pc cm$^{-3}$ (Tendulkar et al. 2017), so we use the average value of 140 pc cm$^{-3}$. We assume that the IGM does not have a significant contribution to the $N_{\mathrm{H}}$, as it is expected to be nearly fully ionized and thus provides negligible X-ray absorption (e.g., Behar et al. 2011; Starling et al. 2013). This Galactic plus host DM of 328 pc cm$^{-3}$ corresponds to $N_{\mathrm{H}} \sim 1 \times 10^{22}$ cm$^{-2}$.

However, such a determination only holds in environments similar to our Galaxy. Photoelectric absorption and dispersion are dominated by separate components of the ISM, namely atomic metals and free electrons, respectively, and their ratios could be significantly different in other environments. To illustrate the effect of excess X-ray absorption, we also consider a case where the $N_{\mathrm{H}}$ is two orders of magnitude higher at $\sim 1 \times 10^{24}$ cm$^{-2}$. At this $N_{\mathrm{H}}$ nearly all of the 0.5–10 keV X-ray flux is absorbed. This situation may be possible in a supernova remnant (SNR) in the first few decades following the supernova, where the ratio of atomic metals to free electrons could be high (Metzger et al. 2017).

For the spectra of the bursts, we assume a few fiducial models. We take a blackbody spectrum with $kT = 10$ keV as a model similar to those observed in magnetar hard X-ray bursts (e.g., Lin et al. 2012; An et al. 2014). We take a cutoff power-law with index $\Gamma = 0.5$ and cutoff energy of 500 keV as a spectrum typical of a magnetar giant flare (Mazets et al. 2005; Palmer et al. 2005, for SGR 1806−20). Finally, we use a power-law model with index $\Gamma = 2$ as an example soft spectrum to contrast with the harder magnetar models.

In Table 3, we give the fluence limits for each of these models and the implied limit on their unabsorbed emitted energy both in the 0.5–10 keV band and extrapolated to the 10 keV–1 MeV gamma-ray band. Note that the energy limits are highly dependent on the amount of absorption and the gamma-ray energy is heavily dependent on the assumed spectrum, as it is extrapolated outside of the 0.5–10 keV band. In Figure 5, we plot each model normalized to its fluence upper limit.

It is clear that assumptions on the underlying spectral model change the implication for the X-ray–gamma-ray luminosity. If the X-ray absorption is increased, the energy limits for the models in Table 3 increase by 1–2 orders of magnitude. Furthermore, a burst that primarily emits energy outside of the 0.5–10 keV soft X-ray band, similar to the magnetar burst and flare models in Table 3, can be much more luminous than in a soft model and be undetectable by *Chandra* and *XMM-Newton*.

When searching for X-rays at the time of radio bursts and placing an associated limit, we are assuming that an X-ray burst is emitted at the same time as each radio burst and that periods of radio burst activity are correlated with X-ray activity. However, if the episodic detection of radio bursts is not intrinsic but due to amplification of the intrinsic emission from lensing by the intervening medium (e.g., Cordes et al. 2017),

6

**Table 2**
Detected Radio Bursts

| Burst No. | Barycentric Arrival Time[a] | Peak Flux Density (Jy) | Fluence (Jy ms) | Gaussian FWHM (ms) | X-Ray Fluence Limit[b] ($10^{-10}$ erg cm$^{-2}$) |
|---|---|---|---|---|---|
| GBT 1 | 57647.232346450619 | 0.36 | 0.82 | 2.16 ± 0.06 | 2 |
| GBT 2 | 57647.232346883015 | 0.08 | 0.16 | 1.94 ± 0.25 | 2 |
| GBT 3 | 57649.173812898174 | 0.36 | 1.32 | 3.45 ± 0.07 | 2 |
| GBT 4 | 57649.218213226581 | 0.29 | 0.34 | 0.88 ± 0.07 | 2 |
| GBT 5 | 57765.049526345771 | 0.17 | 0.33 | 1.40 ± 0.09 | 5 |
| GBT 6 | 57765.064793212950 | 0.38 | 0.83 | 1.79 ± 0.04 | 5 |
| GBT 7 | 57765.069047502300 | 0.20 | 0.62 | 2.97 ± 0.12 | 5 |
| GBT 8[c] | 57765.100827859293 | 0.09 | 0.18 | 2.46 ± 0.28 | 5 |
| GBT 9[c] | 57765.120778204779 | 0.56 | 1.08 | 1.36 ± 0.03 | 5 |
| GBT 10 | 57765.136498608757 | 0.11 | 0.22 | 1.68 ± 0.17 | 5 |
| AO 1[c] | 57765.100827849608 | 0.09 | 0.37 | 4.29 ± 0.11 | 5 |
| AO 2 | 57765.108680842022 | 0.02 | 0.03 | 3.69 ± 0.57 | 5 |
| AO 3[c] | 57765.120778202479 | 0.02 | 0.05 | 4.34 ± 0.44 | 5 |
| AO 4 | 57765.143337535257 | 0.03 | 0.10 | 3.66 ± 0.32 | 5 |

**Notes.**
[a] Corrected for dispersion delay to infinite frequency using DM = 559 pc cm$^{-3}$.
[b] Confidence upper limit. See Section 3.2 for details.
[c] GBT 8/AO 1 and GBT 9/AO 3 are GBT and Arecibo co-detections (see Section 3.1).
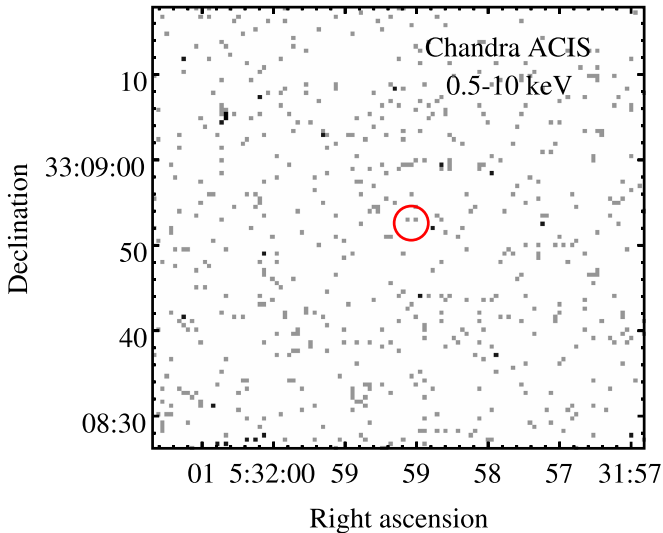


**Figure 4.** Co-added image of all *Chandra* observations of the FRB 121102 field in the 0.5–10 keV range. The red circle of radius 2″ is centered on the position from Marcote et al. (2017).

the detection of radio bursts and X-ray bursts may not be strongly correlated. If the radio bursts are externally amplified, their intrinsic energies could be lower by $\lesssim 10^2$ than what is implied from their detection (Cordes et al. 2017). So, if the intrinsic source of FRBs also produces X-ray emission with a fluence ratio $F_R/F_X$, the expected X-ray emission could be up to two orders of magnitude lower if the radio burst is extrinsically amplified.

### 4.2. Comparison to Previous Limits

For all of the known FRBs at the time, Tendulkar et al. (2016) placed a limit on the fluence ratio defined as $\eta = F_{1.4\,\mathrm{GHz}}/F_\gamma$, where $F_{1.4\,\mathrm{GHz}}$ is the radio fluence at a frequency of 1.4 GHz and $F_\gamma$ is the gamma-ray fluence. The most constraining limit is for FRB 010724 with $\eta > 8 \times 10^8$ Jy ms erg$^{-1}$ cm$^2$. If we assume our fiducial giant flare model

(i.e., cutoff power-law with $\Gamma = 0.5$ and cutoff energy of 500 keV) with $N_{\mathrm{H}} = 10^{22}$ cm$^{-2}$, our gamma-ray fluence limit is $1 \times 10^{-10}$ erg cm$^{-2}$ for a typical photon energy of 20 keV (as in Tendulkar et al. 2016). If we further assume that the 1.4 GHz fluence is approximately the same as the 2 GHz fluence, we can place a lower limit on the ratio of radio-to-gamma-ray fluence of $\eta > 6 \times 10^9$ Jy ms erg$^{-1}$ cm$^2$ for FRB 121102. We can also compare to our *Fermi*/GBM limits, which, though less constraining, do not rely on an extrapolation from soft X-rays into gamma-ray wavelengths. Using this limit the corresponding fluence ratio limit is $\eta > 2 \times 10^8$ Jy ms erg$^{-1}$ cm$^2$.

A gamma-ray burst counterpart to FRB 131104 with energy of $5 \times 10^{51}$ erg has been claimed by DeLaunay et al. (2016), though it has been contested by Shannon & Ravi (2017). The implied radio-to-gamma-ray fluence ratio from the claimed detection is $\eta = 6 \times 10^5$ Jy ms erg$^{-1}$ cm$^2$. DeLaunay et al. (2016) also searched for *Swift*/BAT sub-threshold events at any time *Swift*/BAT was pointed toward the source for 16 FRBs, including FRB 121102, and concluded that there is no evidence for repeated gamma-ray emission from those FRBs above *Swift*/BAT sensitivities. We can nevertheless compare our limits to an event similar to that claimed for FRB 131104. Our limits clearly rule out an event of that magnitude at any time during *XMM-Newton* or *Chandra* observations of FRB 121102. Further, such an event is clearly ruled out from the *Fermi*/GBM limits, both at the time of the bursts and at any time while FRB 121102 is visible to GBM and actively emitting radio bursts.

### 4.3. Models of FRBs

Models of FRBs from magnetars predict a small ratio between the fluence of radio and high-energy emission. Because the radio is a small fraction of the total emitted energy in these models, high-energy emission may be detectable. Based on analogies to solar flares, Lyutikov (2002) estimates a ratio of $10^{-4}$. Lyubarsky (2014) predicts $10^{-5}$–$10^{-6}$ based on a model of a synchrotron maser produced

**Table 3**
Burst Limits for Different X-Ray Spectral Models

| Model | $N_H$ ( cm$^{-2}$) | $kT/\Gamma$ (keV/-) | Absorbed 0.5–10 keV Fluence Limit ($10^{-11}$ erg cm$^{-2}$) | Unabsorbed 0.5–10 keV Energy Limit[a] ($10^{45}$ erg) | Extrapolated 10 keV–1 MeV Energy Limit[a] ($10^{47}$ erg) |
|---|---|---|---|---|---|
| Blackbody | $10^{22}$ | 10 | 5 | 6 | 2 |
| Blackbody | $10^{24}$ | 10 | 13 | 110 | 30 |
| Cutoff PL | $10^{22}$ | 0.5 | 3 | 4 | 13 |
| Cutoff PL | $10^{24}$ | 0.5 | 11 | 120 | 400 |
| Soft PL | $10^{22}$ | 2 | 1.3 | 3 | 0.04 |
| Soft PL | $10^{24}$ | 2 | 8 | 300 | 40 |

**Note.** $5\sigma$ confidence upper limits. See Section 4.1 for details.
[a] Assuming the measured luminosity distance to FRB 121102, 972 Mpc (Tendulkar et al. 2017).
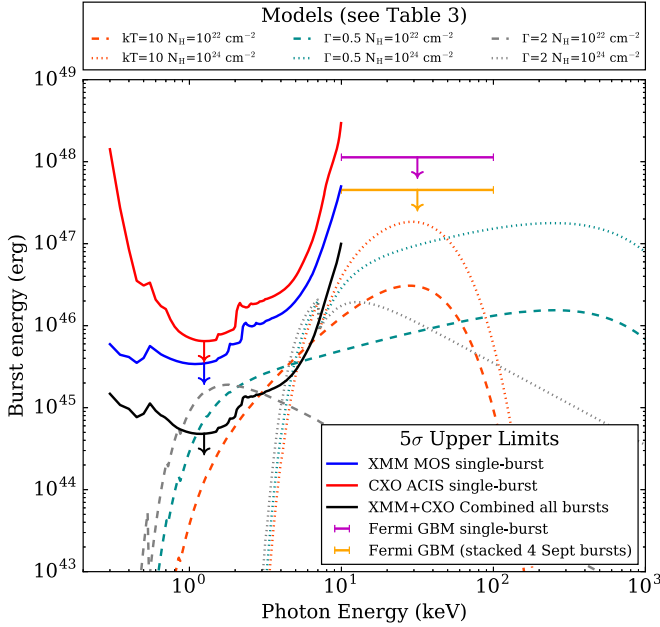


**Figure 5.** Limits on energy of X-ray bursts at the time of radio bursts from FRB 121102. Solid lines show the $5\sigma$ upper limits as a function of X-ray photon energy. The dashed lines show different burst spectra that are photoelectrically absorbed by an $N_H = 10^{22}$ cm$^{-2}$ plotted at their 0.5–10 keV fluence limits that result from a stacked search of the times of the radio bursts. The dotted lines show the same spectral models but with $N_H = 10^{24}$ cm$^{-2}$ to show the effects of absorption. Orange lines represent a blackbody model with $kT = 10$ keV, cyan curves show a cutoff power-law model with $\Gamma = 0.5$ and $E_{cut} = 500$ keV, and the gray curves show a soft power-law with $\Gamma = 2$ in order to illustrate the effect of different spectral models.

from a magnetized shock during magnetar activity. Our X-ray limit implies a radio-to-X-ray ratio of $>10^{-6}$–$10^{-8}$, depending on the spectral model and the absorbing column, which is close to the range where we can begin constraining these models.

We can also compare our limits to the most luminous magnetar giant flare emitted in our Galaxy, that of SGR 1806−20. The 2004 giant flare had a spectrum similar to that of our canonical giant flare in Table 3, a gamma-ray luminosity of $\sim 10^{47}$ erg s$^{-1}$, and a duration of $\sim 100$ ms (Mazets et al. 2005; Palmer et al. 2005). For the $N_H = 1 \times 10^{22}$ cm$^{-2}$ case, this corresponds to a 0.5–10 keV fluence of $\sim 5 \times 10^{-12}$ erg cm$^{-2}$ at the luminosity distance of FRB 121102. This is approximately an order of magnitude lower than our corresponding extrapolated limit.

### 4.4. The Nature of the Persistent Source

Chatterjee et al. (2017) showed that FRB 121102 is associated with a $\sim 0.2$ mJy persistent radio source and Marcote et al. (2017) further showed, using EVN observations, that the persistent source is compact to a projected size of 0.7 pc and consistent with being coincident with the source of the FRB 121102 bursts. Two possible scenarios are considered in Marcote et al. (2017) for the persistent source: an extragalactic neutron star embedded in an SNR, perhaps producing a PWN. Alternatively, an AGN origin is considered. Here, we explore how the limit on X-ray emission from a persistent source at the location of FRB 121102 informs these scenarios.

At the luminosity distance of FRB 121102, 972 Mpc (Tendulkar et al. 2017), no nebula similar to those in our Galaxy would be visible by several orders of magnitude (e.g., the Crab Nebula would have a 0.5–10 keV X-ray flux of $\sim 1 \times 10^{-19}$ erg s$^{-1}$ cm$^{-2}$, well below the sensitivities of current X-ray detectors). However, given the possibility that the radio bursts of FRB 121102 originate from a young neutron star (e.g., Cordes & Wasserman 2016; Katz 2016b; Lyutikov et al. 2016), a nebula resulting from either the supernova that produced the neutron star or a wind driven by either the rotational (PWN) or magnetic (magnetar wind nebula) energy of the young neutron star is an attractive model for the persistent radio source (Metzger et al. 2017).

Given the existence of a luminous persistent radio source at such a distance, one might also expect an exceptionally luminous X-ray source. Taking the Crab Nebula and scaling its X-ray flux by the ratio between its radio luminosity and the radio luminosity of the persistent counterpart to FRB 121102 (a factor of $4 \times 10^5$), we arrive at a 0.5–10 keV X-ray flux of $\sim 5 \times 10^{-14}$ erg s$^{-1}$ cm$^{-2}$. This is over an order of magnitude brighter than the $5\sigma$ limit that we placed in Section 3.4. We can therefore confidently rule out a scaled version of the Crab Nebula. However, such a nebula, powered by a young ($<100$ years) pulsar or magnetar, does not have an analogue in our Galaxy and may therefore have properties different from that of the Crab. Furthermore, in the case that the nebula is a bright X-ray emitter, the soft X-rays may be absorbed by the supernova ejecta (Metzger et al. 2017). For example, assuming a Crab-like X-ray spectrum, our hypothetical "scaled-Crab" nebula would have an absorbed 0.5–10 keV X-ray flux below our $5\sigma$ limit for $N_H \gtrsim 5 \times 10^{23}$ cm$^{-2}$.

The persistent source coincident with FRB 121102 could also plausibly be a massive black hole, resembling the properties observed in low-luminosity active galactic nuclei (LLAGNs). It was shown by Marcote et al. (2017) that the

observed persistent radio emission cannot be explained by either a stellar-mass black hole (such as in X-ray binaries) or an intermediate-mass black hole. On the other hand, the mass of a super-massive black hole is constrained by the stellar mass of the dwarf galaxy (Tendulkar et al. 2017). We would thus expect a black hole mass in the range $\sim 10^5$–$10^7\,M_\odot$.

Considering our upper limit on the X-ray emission (which implies a luminosity of $\lesssim 10^{41}\,erg\,s^{-1}$) and the radio flux density at 5 GHz (Chatterjee et al. 2017; Marcote et al. 2017), we infer a ratio between the radio and X-ray luminosities (Terashima & Wilson 2003) of $\log R_X \gtrsim -2.7$, consistent with the ratio observed in radio-loud AGNs (Ho 2008). This ratio is also consistent with the values of $R_X \sim -2$ observed in radio-loud LLAGNs (Paragi et al. 2012), and so a massive black hole resembling a radio-loud LLAGNs but scaled down in mass remains a plausible model for the persistent radio source.

## 5. Conclusion

Here, we have placed the deepest limits to date on soft (0.5–10 keV) X-ray emission emitted during FRBs as well as from persistent X-ray emission from the location of an FRB source. These limits rule out extreme scenarios but allow many reasonable models. Our limits on the 0.5–10 keV burst energy at the time of radio bursts range from $10^{45}$ to $10^{47}$ erg depending on the underlying model and level of X-ray absorption. We can confidently rule out events with GRB-like energies ($\gtrsim 10^{49}$ erg). Our limits, however, are about an order of magnitude higher than the brightest observed Galactic giant flare, so we do not rule out that model. However, X-ray bursts from possible FRB sources, like magnetars, may emit the majority of their flux at photon energies higher than 10 keV. Pointed hard X-ray/soft gamma-ray observations with telescopes such as *NuSTAR* will therefore be interesting.

Our limit on the persistent luminosity of an X-ray source at the location of the FRB 121102 source is $3 \times 10^{41}\,erg\,s^{-1}$. We showed that if we assume that the persistent radio source at the location of FRB 121102 has a Crab Nebula-like spectrum, it should have been detectable in our X-ray observations. However, such a nebula could be undetectable if there is a high amount of X-ray absorption, or if the nebular spectrum has a higher radio-to-X-ray luminosity ratio than that of the Crab Nebula. We also show that the radio-to-X-ray luminosity ratio limit is consistent with known radio-loud LLAGNs.

More fundamentally, at $\sim$Gpc distances, the fluxes we expect for shorter wavelength (i.e., optical–X-ray–gamma-ray) counterparts are unreachable at millisecond timescales if the energy emitted at those wavelengths is comparable to the emitted radio energy of FRBs. Therefore, if an event that produces an FRB emits a large fraction of its energy at radio wavelengths, we would not expect multi-wavelength burst counterparts to be detectable. However, we must place the most stringent limits possible in case the converse—that the radio emission is a small fraction of the total emitted energy—is true. Such limits therefore inform possible models of FRBs. In the future, with instruments that promise to detect large numbers of FRBs (e.g., CHIME, UTMOST, DSA-10, ALERT), we may accumulate a sample of relatively nearby ($\lesssim 100$ Mpc), bright, repeating FRBs that would be more likely to have detectable high-energy burst counterparts.

### ORCID iDs

P. Scholz ⓘ https://orcid.org/0000-0002-7374-7119
S. Bogdanov ⓘ https://orcid.org/0000-0002-9870-2742
J. W. T. Hessels ⓘ https://orcid.org/0000-0003-2317-1446
R. S. Lynch ⓘ https://orcid.org/0000-0001-5229-7430
G. C. Bower ⓘ https://orcid.org/0000-0003-4056-9982
S. Burke-Spolaor ⓘ https://orcid.org/0000-0003-4052-7838
J. M. Cordes ⓘ https://orcid.org/0000-0002-4049-1882
V. M. Kaspi ⓘ https://orcid.org/0000-0001-9345-0307
C. J. Law ⓘ https://orcid.org/0000-0002-4119-9963
B. Marcote ⓘ https://orcid.org/0000-0001-9814-2354
M. A. McLaughlin ⓘ https://orcid.org/0000-0001-7697-7422
Z. Paragi ⓘ https://orcid.org/0000-0002-5195-335X
S. M. Ransom ⓘ https://orcid.org/0000-0001-5799-9714
S. P. Tendulkar ⓘ https://orcid.org/0000-0003-2548-2926

# References

An, H., Kaspi, V. M., Beloborodov, A. M., et al. 2014, ApJ, 790, 60
Bannister, K. W., Shannon, R. M., Macquart, J.-P., et al. 2017, ApJL, 841, L12
Barr, E. D., Champion, D. J., Kramer, M., et al. 2013, MNRAS, 435, 2234
Bassa, C. G., Tendulkar, S. P., Adams, E. A. K., et al. 2017, ApJL, 843, L8
Behar, E., Dado, S., Dar, A., & Laor, A. 2011, ApJ, 734, 26
Caleb, M., Flynn, C., Bailes, M., et al. 2017, MNRAS, 468, 3746
Chatterjee, S., Law, C. J., Wharton, R. S., et al. 2017, Natur, 541, 58
Cordes, J. M., Freire, P. C. C., Lorimer, D. R., et al. 2006, ApJ, 637, 446
Cordes, J. M., & Lazio, T. J. W. 2002, arXiv:astro-ph/0207156
Cordes, J. M., & Wasserman, I. 2016, MNRAS, 457, 232
Cordes, J. M., Wasserman, I., Hessels, J. W. T., et al. 2017, ApJ, 842, 35
DeLaunay, J. J., Fox, D. B., Murase, K., et al. 2016, ApJL, 832, L1
DuPlain, R., Ransom, S., Demorest, P., et al. 2008, Proc. SPIE, 7019, 70191D
Falcke, H., & Rezzolla, L. 2014, A&A, 562, A137
Fruscione, A., McDowell, J. C., Allen, G. E., et al. 2006, Proc. SPIE, 6270, 62701V
He, C., Ng, C.-Y., & Kaspi, V. M. 2013, ApJ, 768, 64
Ho, L. C. 2008, ARA&A, 46, 475
Kashiyama, K., Ioka, K., & Mészáros, P. 2013, ApJL, 776, L39
Kashiyama, K., & Murase, K. 2017, ApJL, 839, L3
Katz, J. I. 2016a, MPLA, 31, 1630013
Katz, J. I. 2016b, ApJ, 826, 226
Kraft, R. P., Burrows, D. N., & Nousek, J. A. 1991, ApJ, 374, 344
Law, C. J., Abruzzo, M. W., Bassa, C. G., et al. 2017, ApJ, submitted, arXiv:1705.07553
Lazarus, P., Brazier, A., Hessels, J. W. T., et al. 2015, ApJ, 812, 81
Lin, L., Göğüş, E., Baring, M. G., et al. 2012, ApJ, 756, 54
Lorimer, D. R., Bailes, M., McLaughlin, M. A., Narkevic, D. J., & Crawford, F. 2007, Sci, 318, 777

Lunnan, R., Chornock, R., Berger, E., et al. 2014, ApJ, 787, 138
Lyubarsky, Y. 2014, MNRAS, 442, L9
Lyutikov, M. 2002, ApJL, 580, L65
Lyutikov, M., Burzawa, L., & Popov, S. B. 2016, MNRAS, 462, 941
Marcote, B., Paragi, Z., Hessels, J. W. T., et al. 2017, ApJL, 834, L8
Masui, K., Lin, H.-H., Sievers, J., et al. 2015, Natur, 528, 523
Mazets, E. P., Cline, T. L., Aptekar, R. L., et al. 2005, arXiv:astro-ph/0502541
Meegan, C., Lichti, G., Bhat, P. N., et al. 2009, ApJ, 702, 791
Metzger, B. D., Berger, E., & Margalit, B. 2017, ApJ, 841, 14
Palmer, D. M., Barthelmy, S., Gehrels, N., et al. 2005, Natur, 434, 1107
Paragi, Z., Shen, Z. Q., de Gasperin, F., et al. 2012, in Proc. 11th European VLBI Network Symp. and Users Meeting 8, ed. P. Charlot, G. Bourda, & A. Collioud (Trieste: SISSA), 8
Pen, U.-L., & Connor, L. 2015, ApJ, 807, 179
Petroff, E., Barr, E. D., Jameson, A., et al. 2016, PASA, 33, e045
Popov, S. B., & Postnov, K. A. 2013, arXiv:1307.4924
Ransom, S. M. 2001, PhD thesis, Harvard Univ.
Scholz, P., Spitler, L. G., Hessels, J. W. T., et al. 2016, ApJ, 883, 177
Shannon, R. M., & Ravi, V. 2017, ApJL, 837, L22
Spitler, L. G., Cordes, J. M., Hessels, J. W. T., et al. 2014, ApJ, 790, 101
Spitler, L. G., Scholz, P., Hessels, J. W. T., et al. 2016, Natur, 531, 202
Starling, R. L. C., Willingale, R., Tanvir, N. R., et al. 2013, MNRAS, 431, 3159
Tendulkar, S. P., Bassa, C. G., Cordes, J. M., et al. 2017, ApJL, 834, L7
Tendulkar, S. P., Kaspi, V. M., & Patel, C. 2016, ApJ, 827, 59
Terashima, Y., & Wilson, A. S. 2003, ApJ, 583, 145
Thornton, D., Stappers, B., Bailes, M., et al. 2013, Sci, 341, 53
Verner, D. A., Ferland, G. J., Korista, K. T., & Yakovlev, D. G. 1996, ApJ, 465, 487
Wilms, J., Allen, A., & McCray, R. 2000, ApJ, 542, 914
Yao, J. M., Manchester, R. N., & Wang, N. 2017, ApJ, 835, 29
Younes, G., Kouveliotou, C., Huppenkothen, D., et al. 2016, ATel, 8781, 1